Synthetic Essentiality of Tryptophan 2,3-dioxygenase 2 in APC-Mutated Colorectal Cancer

Rumi Lee[1], Jiexi Li[1], Jun Li[2], Chang-Jiun Wu[2], Shan Jiang[4], Wen-Hao Hsu[1], Deepavali Chakravarti[1], Peiwen Chen[1], Kyle A. LaBella[1], Jing Li[5], Denise J. Spring[1], Di Zhao[1,3], Y. Alan Wang[1*], and Ronald A. DePinho[1*]

Affiliations:

[1]Department of Cancer Biology, The University of Texas MD Anderson Cancer Center, Houston, TX 77030, USA

[2]Department of Genomic Medicine, The University of Texas MD Anderson Cancer Center, Houston, TX 77030, USA

[3]Department of Experimental Radiation Oncology, The University of Texas MD Anderson Cancer Center, Houston, TX 77030, USA

[4]Department of The Translational Research to AdvanCe Therapeutics and Innovation in ONcology (TRACTION), The University of Texas MD Anderson Cancer Center, Houston, TX 77030, USA

[5]Karmanos Cancer Institute, Department of Oncology, Wayne State University School of Medicine, Detroit, MI 48201, USA

Running title

Synthetic Essentiality of TDO2 in APC-Mutated CRC

Keywords

APC, TDO2, CXCL5, Tumor-associated macrophages, Colorectal cancer

Additional Information

Funding: This work was supported by MD Anderson SPORE in Gastrointestinal Cancer (R.A.D.), NIH/NCI R01 CA231360 (R.A.D.) and NIH/NCI 1R01 CA231349 (Y.A.W.). R.L. was supported by NIH T32 Training Grant in Cancer Biology (T32 CA186892; R. Kalluri). Jiexi Li and W-H.H. were supported by the CPRIT Research Training Program (RP170067). K.A.L. was supported by a training fellowship from UT Health Science Center at Houston Center for Clinical and Translational Sciences TL1 Program (TL1 TR003169). D.Z. was supported by CPRIT Recruitment of First-Time Tenure-Track Faculty Award RR190021 (CPRIT Scholar in Cancer Research). The Flow Cytometry and Cellular Imaging Core at MD Anderson Cancer Center is partially funded by NCI Cancer Center Support Grant P30 CA16672. The metabolomic profiling was done in the Pharmacology and Metabolomics Core at Karmanos Cancer Institute, which is supported, in part, by the United States Public Health Service Cancer Center Support Grant P30 CA022453.

***Corresponding authors**: Ronald A. DePinho, Department of Cancer Biology, University of Texas MD Anderson Cancer Center, 1515 Holcombe Blvd, Unit 1906,

Houston, Texas 77030 USA; Tel: +1-832-751-9756; E-mail: RDePinho@mdanderson.org; and Y. Alan Wang, Tel: +1-713-792-7928; E-mail: yalanwang@mdanderson.org

Conflict of Interest: R.A.D. is the Founder and Advisor for Tvardi Therapeutics, Asylia Therapeutics, Stellanova Therapeutic, Nirogy Therapeutics and Sporos Bioventures; The work of this paper was performed in the laboratory of R.A.D. and not linked to these biotechnology companies.

Abstract

Inactivation of the adenomatous polyposis coli (APC) is common across many cancer types and serves as a critical initiating event in most sporadic colorectal cancers (CRC). APC-deficiency activates WNT signaling which remains an elusive target for cancer therapy, prompting us to apply the synthetic essentiality framework to identify druggable vulnerabilities for APC-deficient cancers. Tryptophan 2,3-dioxygenase 2 (TDO2) was identified as a synthetic essential effector of APC-deficient CRC. Mechanistically, APC-deficiency results in TCF4/ β-catenin-mediated upregulation of TDO2 gene transcription. TDO2 in turn activates the Kyn-AhR pathway which increases glycolysis to drive anabolic cancer cell growth and CXCL5 secretion to recruit macrophages into the tumor microenvironment. Therapeutically, APC-deficient CRC models were susceptible to TDO2 depletion or pharmacological inhibition which impaired cancer cell proliferation and enhanced anti-tumor immune profiles. Thus, APC-

deficiency activates a TCF4-TDO2-AhR-CXCL5 circuit that impacts multiple cancer hallmarks via autonomous and non-autonomous mechanisms, and illuminates a genotype-specific vulnerability in CRC.

Statement of Significance (50-word limit)

This study identifies critical effectors in the maintenance of APC-deficient CRC and demonstrates the relationship between APC/WNT pathway and kynurenine pathway signaling. It further determines the tumor-associated macrophage biology in APC-deficient CRC, informing genotype-specific therapeutic targets and the use of TDO2 inhibitors.

Introduction

CRC is the second leading cause of cancer-related death in developed countries, causing more than 600,000 deaths globally each year. The evolution of CRC from adenoma to adenocarcinoma and ultimately invasive and metastatic disease is governed by the acquisition of signature genetic alterations, most prominently inactivation of APC and p53 tumor suppressors and activation of the KRAS oncogene (1). Loss of APC is considered the critical initiating event, occurring in the vast majority (~90%) of sporadic CRC. Consistent with its gatekeeper role, ApcMin/+ mice harboring a mutated APC gene develop adenomatous polyps throughout the intestine (2). CRC mouse models have also established an essential role for APC-deficiency in tumor maintenance (3).

APC loss occurs frequently across many cancer types (4-7), motivating efforts to identify key APC signaling surrogates essential for tumor maintenance. In normal cells,

APC activates glycogen synthase kinase 3β (GSK3β) which in turn phosphorylates N-terminal serine/threonine residues of β-catenin, mediating β-catenin degradation through ubiquitination. Thus, APC-deficient cancers accumulate β-catenin which then translocates to the nucleus to bind and de-repress the T cell factor/lymphoid enhancer factor (TCF/LEF) transcription factor complex (8), enabling activation of the canonical WNT signaling network.

Despite its importance in cancer, the therapeutic targeting of this WNT/APC signaling cascade remains an elusive goal for cancer therapy. Currently, agents targeting WNT pathway include inhibitors of WNT ligands, β-catenin degrading complex, TCF/LEF, and Notch and Sonic Hedgehog signaling which crosstalk with WNT. To date, these WNT targeting programs have yet to produce meaningful clinical results, motivating us to adopt an orthogonal strategy to identify key downstream effectors of APC-deficiency needed for tumor maintenance. To that end, we adopted the synthetic essentiality (SE) approach which begins with a search for genes that can be occasionally mutated/deleted in cancers but are never or rarely deleted in cancers harboring loss of a specific tumor suppressor gene. These mutually exclusive patterns in the cancer genome might merely belie an epistatic relationship or indicate that the SE gene serves as an essential effector of the specific tumor suppressor gene deficiency in supporting tumorigenesis. The first validated example of SE was chromatin helicase DNA-binding factor (CHD1) which serves as an essential effector of PTEN-deficiency in prostate and breast cancers (9).

In the current study, the SE approach (10) identified Tryptophan 2,3-dioxygenase 2 (TDO2) as a key downstream effector specifically in APC-deficient CRC. TDO2

mediates the first and rate-limiting step of the kynurenine pathway (KP), the major tryptophan (Trp) catabolism pathway in mammals and converts Trp into N-formylkynurenine (Kyn). TDO2 is highly expressed and constitutively active in diverse cancers, which results in the accumulation of Kyn in the tumor microenvironment (TME) to suppress anti-tumor immunity. Trp depletion and Kyn accumulation promote differentiation of monocytes into immunosuppressive tumor-associated macrophages (TAMs) and inhibit T cell proliferation/activation (11). TDO2-Kyn also mediates cancer cell intrinsic pathways through Kyn action as an agonist for aryl hydrocarbon receptor (AhR) which upregulates pro-tumorigenic genes in glioblastoma and triple-negative breast cancer (12, 13). However, the genotypic context in which TDO2 (and by extension other KP enzymes, IDO1 and IDO2) might serve critical rate-limiting roles in specific cancers is not known. Our studies establish that the TDO2-Kyn-AhR axis serves a critical role in promoting APC-deficient tumor growth via cancer cell autonomous (metabolism and proliferation) and non-autonomous mechanisms (tumor immunity).

Results

Identification of TDO2 as a downstream effector for APC deficiency in cancer. To identify synthetic essential effectors of APC-deficiency, we first searched for genes showing mutually exclusive mutation/deletion patterns with APC in The Cancer Genome Atlas (TCGA) database (Supplementary Table S1). To overcome the limitation that only a small fraction of CRC cases are intact for APC, we conducted a pan-cancer analysis that showed consistent retention of TDO2 in APC deleted/mutated cancers

including CRC, breast cancer, prostate cancer, lung cancer, head and neck squamous cell carcinoma and sarcoma (Supplementary Fig. S1A). Recognizing the limited sample size and low frequency of these genomic events, we triangulated these genomic results with (i) hits from genome wide loss-of-function screens designed to identify genes that are consistently retained in cancer cells bearing APC loss-of-function mutations (14) and (ii) unbiased transcriptomic analyses to identify genes with positive correlations of WNT pathway activation signature (15) and HALLMARK_WNT_BETA_CATENIN_SIGNALING (16). These intersections yielded 5 potential SE genes for APC-deficient tumors (TDO2, C3, MAFB, CAB39L, PPFIA2) with TDO2 as the top hit (Fig. 1A).

Analysis of human TCGA CRC datasets (COAD and READ) revealed that TDO2 gene expression indeed correlated positively with WNT pathway activation (Fig. 1B and Supplementary Fig. S1, B-D). Correspondingly, tumor microarray analysis of human CRC samples showed coincident increased signal for TDO2 and for nuclear β-catenin and c-Myc, which are indicative of WNT pathway activation (Fig. 1C and D, Supplementary Fig. S1, E-H). In murine models, CRC tumors of iAP mice ($APC^{mut}/TP53^{mut}$) and iKAP mice (inducible $Kras^{mut}$ with $APC^{mut}/TP53^{mut}$) (17) showed that TDO2 expression tracks closely with β-catenin and Ki67 signals in tumors (Fig. 1E and Supplementary Fig. S1I). Finally, $Apc^{Min/+}$ organoids and RISPR/Cas9-mediated APC-KO organoids showed significantly increased TDO2 expression compared to APC-WT organoids (Fig. 1, F and G).

In contrast, another KP enzyme, IDO1, did not exhibit mutual exclusive patterns with APC and CTNNB1 mutations in TCGA CRC nor correlate with WNT pathway

activation. IDO2 expression exhibited a correlation with WNT signaling, although its baseline expression level was extremely low (Supplementary Fig. S1, J-L). Collectively, APC-deficiency correlates with increased TDO2 expression in normal and malignant intestinal epithelium in humans and mice.

APC-deficiency upregulates TDO2 expression via TCF4. Increased TDO2 mRNA levels upon APC deletion in isogenic cells (Fig 2, A and B, Supplementary Fig. S2A) prompted examination of the human and mouse TDO2 gene promoter region for transcription factors using JASPAR and ECR Browser transcription factor binding profile databases. A conserved WNT pathway transcription factor binding element for TCF4/TCF7L2 was identified immediately upstream of the human and mouse TDO2 transcription start sites (Fig. 2C). ChIP-seq confirmed TCF4 binding in the TDO2 promoter of APC-KO but not APC-WT MC38 cells (Fig. 2D). In the human APC-null DLD1 cell line, ChIP-PCR also documented TCF4 binding to the promoters of TDO2 and the classical WNT target genes AXIN2 and MYC, but not GAPDH promoter which served as a negative control (Fig. 2E). Furthermore, a luciferase reporter driven by the human TDO2 promoter showed increased reporter activity upon transduction of constitutively active β-catenin (CTNNB1 Δ90), which mimics WNT pathway activation (Fig. 2F). Conversely, dominant-negative TCF4 expression or TCF4 binding motif mutation abrogated reporter activity (Fig. 2, G and H). Finally, TCF4 depletion or WNT inhibitor XAV-939 treatment, which destabilizes β-catenin, decreased TDO2 levels in multiple independent WNT-activated cells (Fig. 2I, Supplementary Fig. S2, B-I). Thus, APC loss activates WNT-β-catenin resulting in TCF4-mediated upregulation of TDO2 gene transcription.

TDO2 depletion specifically impairs the growth and survival of APC/WNT-mutated CRC cells. To assess TDO2 essentiality as a function of APC status, the biological impact of TDO2 depletion or pharmacological inhibition was tested across multiple murine and human models. Using validated shRNAs (Supplementary Fig. S3A), TDO2 depletion had no impact on colony formation of human APC-WT RKO cells yet impaired colony formation of isogenic CRISPR/Cas9-generated APC-null RKO controls (Supplementary Fig. S3, B and C). Similarly, multiple human APC/CTNNB1-mutant CRC lines (DLD1, LS180, HT-29, Caco-2) (Supplementary Fig. S3D) showed markedly reduced colony formation upon TDO2 depletion (Supplementary Fig. S3, B and C). Correspondingly, TDO2-specific inhibitor 680C91 (18) treatment impaired the growth and survival of APC-deficient but not APC-WT cancer cells including primary CCD-841-CoN colon epithelial cells (Supplementary Fig. S3, E and F). In murine cell models, both TDO2 depletion and pharmacological inhibition impaired the growth and cell death of APC-null MC38 cells but not the parental APC-WT controls (Fig. 3, A-C, Supplementary Fig. S3, G-I). Similarly, shRNA-mediated TDO2 depletion in cultured $Apc^{Min/+}$ intestinal organoids induced cell death and pharmacological inhibition of TDO2 induced inhibited the growth APC-KO intestinal organoids, but not APC-WT controls (Fig. 3, D and E).

In tumor models, TDO2 depletion decreased growth of orthotopic APC-null RKO tumors in immune deficient NSG mice (Supplementary Fig. S4A). Similarly, TDO2 depletion decreased growth of APC-null DLD-1 tumors which was rescued by enforced expression of a hairpin-resistant TDO2 ORF (Supplementary Fig. S4B). Pathological analysis of these TDO2-depleted tumors revealed decreased cancer cell proliferation (Ki67) and increased apoptosis (cleaved Caspase-3), indicating that TDO2 drives these

cancer cell-intrinsic hallmarks (Supplementary Fig. S4, C and D). Similarly, using immune competent mice, TDO2 depletion impaired orthotopic tumor growth, decreased cancer cell proliferation, and increased cancer cell apoptosis (Fig. 3F, Supplementary S4, E and F), and resulted in prolonged overall survival specifically in murine APC-KO MC38, but not APC-WT controls (Fig. 3G). In immune-deficient mice, APC-KO MC38 tumor produced similar survival curves to those in immune competent mice but showed reduced survival benefit from induction of TDO2 depletion, consistent with cancer cell intrinsic and immune modulatory roles for TDO2 specifically in APC-null cancers (Supplementary Fig. S4G).

The recent failure of the IDO inhibitors in CRC trials (19) prompted us to compare the impact of TDO2 and IDO inhibition in our model system. The recently developed validated TDO2 inhibitor PF06845102/EOS200809 (20) was administrated by oral gavage to mice bearing APC-WT or APC-KO MC38 orthotopic tumors. TDO2 inhibitor treatment improved the survival of mice bearing APC-KO MC38 tumors but not APC-WT controls (Fig. 3H). Histopathology showed that TDO2 inhibitor treatment decreased Ki67 and increased cleaved caspase-3 signals specifically in the APC-KO MC38 tumors (Supplementary Fig. S4H). Consistent with the IDO inhibitor failures, the IDO inhibitor, Epacadostat, did not exhibit anti-tumor activity in mice bearing either APC-WT or APC-KO MC38 CRC orthotopic tumors (Supplementary Fig. S4I). Finally, we confirmed the survival benefit of TDO2 inhibitor treatment in autochthonous established tumors arising in the iAP mouse model of CRC. Specifically, tumor-bearing iAP mice, treated with TDO2 inhibitor three weeks following OHT-injection into the colon wall, showed

significant survival benefit compared to vehicle-treated mice (Fig. 3I). Together, these data support the view that TDO2 supports tumor growth specifically in APC-null CRC.

TDO2-Kyn-AhR axis supports APC-deficient cancer cell proliferation, survival and tumorigenic potential. As noted, TDO2 metabolizes Trp to produce Kyn which in turn activates AhR to upregulate genes governing myriad cellular functions. GSEA of isogenic APC-KO and APC-WT MC38 cell lines showed that Dox-induction of inducible shTDO2 decreased signatures of tryptophan metabolism as well as xenobiotic metabolism, patterns consistent with the main functions of the AhR pathway (Supplementary Fig. S5A). Correspondingly, expression of AhR and its target gene CYP1B1 correlated positively with TDO2 levels in TCGA COAD dataset (Supplementary Fig. S5B). CRC tumors from iAP and iKAP also showed that AhR expression strongly tracks with nuclear β-catenin and Ki67 (Supplementary Fig. S5C). Moreover, the APC-KP connection was verified in the APC-KO MC38 model system via ELISA which documented elevated Kyn secretion relative to APC-WT controls (Supplementary Fig. S5D) and TDO2 depletion in APC-KO cells and $Apc^{Min/+}$ organoids reduced Kyn levels (Supplementary Fig. S5, D and E). Finally, gene expression analysis showed upregulated AhR and its downstream genes in APC-KO MC38 cells compared to APC-WT MC38 cells, which was reversed upon TDO2 depletion in APC-KO MC38 cells and DLD1 cell lines (Supplementary Fig. S5, F and G).

To validate Kyn and AhR in mediating TDO2-regulated biology, we assayed the impact of Kyn treatment or AhR depletion in colony formation assays using the APC-KO MC38 ishTDO2 cell lines and APC-KO MC38 shAhR cell lines. In APC-KO MC38 cells, reduced colony formation upon induction of TDO2 depletion or pharmacological

inhibition (680C91) was partially rescued by Kyn treatment (Supplementary Fig. S5, H-L). In the iKAP model system, Kyn treatment also decreased 680C91-induced cell death (Supplementary Fig. S5M). Finally, AhR depletion in APC-KO MC38 tumors resulted in increased survival with corresponding decreased proliferation (Ki67) and survival (Caspase-3) in the cancer cells (Supplementary Fig. S5, N and O). Together, these findings are consistent with a key role for Kyn and AhR as mediators of TDO2 in APC-null cancer cell proliferation, survival, and tumorigenic potential.

TDO2 promotes cancer cell glycolysis and tumor associated macrophage recruitment. To discern the cancer hallmarks regulated by TDO2, GSEA was conducted on APC-KO MC38 cell lines and derivative tumors following TDO2 depletion. Consistent with known cancer cell intrinsic functions of the APC/WNT pathway (21), hypoxia and glycolysis pathways were up-regulated in APC-KO cells (Fig. 4A and Supplementary Fig. S6A). Correspondingly, APC-KO MC38 cells exhibited higher sensitivity to the GLUT1 inhibitor, STF-31, than APC-WT controls (Supplementary Fig. S6B) and showed increased glucose uptake and lactate secretion, which were reversed by TDO2 depletion (Supplementary Fig. S6, C and D). Glycolytic flux Seahorse analysis showed that enforced TDO2 expression increased the key parameters of glycolytic flux which are glycolysis, glycolytic capacity, glycolytic reserve, as well as non-glycolytic acidification, relative to the MC38 empty vector controls, reinforcing the role of TDO2 in promoting glycolysis (Supplementary Fig. S6, E-G). Metabolite analysis of cell lysates and conditioned media from APC-KO MC38 cells showed decreased levels of glycolysis pathway-related metabolites upon TDO2 depletion (Supplementary Fig. S6H). To reinforce the link between TDO2 and the regulation of metabolic pathways, we

examined multiple elements in the GCN2 and mTOR pathways in MC38 APC-WT and APC-KO cells containing an inducible shTDO2 construct. APC deletion increased the level of phosphorylated eIF2, and this increase was reversed upon TDO2 depletion in APC null cells. In addition, TDO2 depletion decreased phosphorylated mTOR, only in the APC null cells (Supplementary Fig. S6I). Finally, RT-PCR analysis confirmed up-regulation of key glycolysis genes (SLC2A1, HK1/2, and PFKL), which were down-regulated upon TDO2 or AhR depletion (Supplementary Fig. S6, J and K). Together, these experimental data show that TDO2-AhR signaling plays a key role in promoting cancer cell glycolysis.

In addition to cancer cell-intrinsic processes, we observed that APC status (APC-KO versus APC-WT MC38) or TDO2 depletion in APC-deficient cancer cells and tumors resulted in prominent representation of immune signaling signatures such as TNFA signaling, inflammatory response, IL-6_JAK_STAT, allograft rejection, and complement (Fig. 4, A and B). These in silico observations prompted immunoprofiling of orthotopic tumors generated from isogenic APC-KO and APC-WT MC38 cells with and without TDO2 depletion. viSNE plots of CyTOF data showed that APC deficiency resulted in significantly increased macrophage abundance, which decreased upon TDO2 depletion (Fig. 4C). Polyps in $Apc^{Min/+}$ mice also showed increased F4/80+ macrophage infiltration (Supplementary Fig. S7A). Quantification of $CD11b^{+}F4/80^{+}$ macrophages and $CD11b^{+}F4/80^{+}$ $CD206^{high}$ M2-like macrophages in CD45-positive population confirmed enrichment of macrophages in APC-KO tumors and their reduction upon TDO2 depletion (Fig. 4D). Immunohistochemistry staining of F4/80 and CD163 in these tumors, as well as the orthotopic tumors treated with TDO2 inhibitor PF06845102/EOS200809,

aligned with the aforementioned CyTOF data (Supplementary Fig. S7, B and C). In contrast, Epacadostat treatment did not increase infiltration of total and M2-like macrophages. (Supplementary Fig. S7C). Comparative transcriptomic analysis of TAMs isolated from APC-WT and APC-KO MC38 tumors express higher levels of multiple classical M2-like markers (CD163, CCL22, YM1) compared to APC-WT tumors (Supplementary Fig. S7, D and E). Interestingly, IHC analysis of APC-WT and APC-KO MC38 tumors confirmed that (i) loss of APC results in decreased CD8-positive cells, (ii) TDO2 inhibition increased the number of infiltrating CD8-positive cells in APC-KO tumors relative to APC-WT controls, and (iii) IDO inhibition is unable to increase CD8-positive cells in the APC-KO tumors (Supplementary Fig. S7F). Evaluation of the activity state of CD8+ T cells in APC-WT and APC-KO MC38 tumors by immune-co-staining of CD8 and activation marker granzyme B showed higher number of activated T cells in APC-KO MC38 tumors compared to APC-WT tumors (Supplementary Fig. S7G).

To corroborate TDO2-mediated TME modulation, TCGA CRC datasets were examined for expression of macrophage (total and M2) as well as Tregs and MDSC markers, revealing strong positive correlations between the degree of WNT activation and TDO2 expression levels (Fig. 4E and Supplementary Fig. S7, H and I). This WNT-macrophage correlation was further validated by human CRC tumor microarray (TMA) analyses which showed that cancer cells with nuclear β-catenin signal exhibited higher CD163 expression in the TME (Fig. 4, F and G). Together, these findings support the model that activated WNT-driven upregulation of TDO2 expression in turn activates the AhR network which functions to recruit immune suppressive TAMs into the TME.

TDO2-AhR-CXCL5 promotes tumor growth by recruiting TAMs into the CRC TME. To identify WNT-TDO2-AhR-regulated factors that may recruit TAMs, we performed cytokine array profiling of conditioned media (CM) from APC-KO MC38 ishTDO2 cells. Induction of TDO2 depletion reduced secretion of classical macrophage cytokines including G-CSF, GM-CSF, CXCL2 (Supplementary Fig. S8A) and other cytokines (see below). Correspondingly, transwell migration assays using bone marrow-derived macrophages (BMDM) showed that CM from APC-KO MC38 ishTDO2 cultures increased macrophage migration which was nullified upon TDO2 depletion (Supplementary Fig. S8, B and C).

Next, to more fully vet the most highly regulated cytokines in our system, we identified and qRT-PCR validated the top ranked genes in the RNA-seq dataset and found that CXCL5, CXCL7 (PPBP), CSF3 (G-CSF), CXCR2, CXCL2, CXCL10, CCL2, and CXCL1 showed the most significant expression changes associated APC deletion or TDO2 depletion (Fig. 5A). To further identify the target cytokines of TDO2, cell lines that express ORFs of the top three genes from RNA-seq data -- CXCL5, CXCL7 (PPBP), and CSF3 -- were generated in APC-KO MC38 ishTDO2 cells and monitored for tumor growth to identify genes that rescue the impaired proliferation by TDO2 knockdown. Enforced expression of CXCL5, which showed the highest fold changes, was most active in rescuing the decreased tumor growth mediated by TDO2 depletion (Fig. 5B). Moreover, CyTOF analysis of CXCL5-overexpressing APC-KO tumors showed increased TAMs in the presence of shTDO2 (Fig. 5, C-E).

Migration assays showed rescue of macrophage recruitment when CM from APC-KO TDO2-depleted MC38 cells was supplemented with CXCL5 whereas co-

treatment with CXCR1/2 inhibitor (SX-682), to which CXCL5 binds, abrogated the rescue by CXCL5 supplementation (Fig. 5F). In addition, AhR inhibitor treatment (CH223191) profoundly decreased CXCL5 expression in APC-KO MC38 cells (Supplementary Fig. S8D). Moreover, BMDMs co-cultured with Kyn or CXCL5 showed increased M2 macrophage marker expression, supporting a role for the TDO2-AhR axis in promoting TAM polarization (Supplementary Fig. S8E).

Immunohistochemical analysis of macrophage markers showed increased infiltration of macrophages in tumors with enforced CXCL5 expression (Supplementary Fig. S8F). To validate the roles of CXCL5 in promoting tumor growth in vivo, we co-injected CT26 cell line and Raw 264.7 macrophage cells that were pre-treated with recombinant CXCL5 proteins and CXCL5-treated macrophages promoted the growth of CT26 significantly (Supplementary Fig. S8G). Finally, allograft mice with APC-KO MC38 cells showed increased survival upon TDO2 or macrophage depletion (Fig. 5G). CXCL5 overexpression in APC-KO MC38 cell lines significantly shortened the survival of mice, which was reversed by depleting macrophages (Fig. 5G). APC-KO MC38 cells treated with anti-CXCL5 neutralizing antibody also showed prolonged survival (Supplementary Fig. S8H).

To further validate the relationship between the TDO2-AhR-CXCL5 axis and TAM abundance in human CRC, TCGA CRC (COAD and READ) dataset was clustered based on CXCL5 expression and analyzed for immune populations. These analyses revealed that TAM abundance correlated positively with high CXCL5 expression (Supplementary Fig. S8, I and J). In addition, CXCL5 expression correlated positively with increased tryptophan metabolism (TDO2 as top pathway signature gene) and

xenobiotic metabolism in TCGA CRC (Supplementary Fig. S8, K-M). Together, these data establish that TDO2-AhR signaling upregulates CXCL5 which recruits TAMs to promote tumor growth; conversely, neutralization of the TDO2-AhR-CXCL5 pathway is a validated anti-tumor strategy in APC null CRC.

Discussion

In this study, we identified TDO2 as a synthetic essential effector in the maintenance of APC-deficient cancers. Increased TDO2 activates the kynurenine pathway (KP) to generate excessive Kyn, which activates AhR network. Genetic and pharmacological interventions established that this TDO2-Kyn-AhR axis increases APC-deficient CRC cancer cell glycolysis, promotes cancer cell proliferation and survival, and upregulates CXCL5 to recruit TAMs into the TME (Fig. 6). In preclinical models, APC-deficient CRC exhibited hypersensitivity to TDO2 inhibition, but not to the IDO1 inhibitor, providing a responder hypothesis for further testing of these immune-modulatory agents in CRC clinical trials. Importantly, iAP mice, engineered with conditional null alleles of *APC* and *TP53*, were induced to develop CRC; subsequent administration of a TDO2 inhibitor increased survival. Together with correlative clinico-pathological profiles of human CRC, these experimental findings establish TDO2 as a potential therapeutic target for APC-null CRC.

Recent studies have revealed TDO2 overexpression in multiple cancer types and its role in facilitating tumorigenic signaling via KP (12, 22, 23). Another key KP enzyme, IDO1, is also highly expressed in various tumors and is known to suppress anti-tumor immunity. However, these functionally related KP enzymes, IDO1 and TDO2, appear to

operate in non-redundant, context-specific settings and are differentially regulated. Specifically, AhR can regulate IDO1, but not TDO2, expression (24). In contrast, transcriptional regulatory mechanisms governing TDO2, but not IDO1, expression include hemes and glucocorticoid hormones (25), as well as the WNT transcription factor TCF4 specifically in APC-deficient CRC cells (this study).

With respect to tumor biology, the TDO2-Kyn-AhR axis regulates glycolysis as a cancer cell intrinsic mechanism, a finding that aligns with previous work showing AhR-mediated regulation of metabolism genes controlling lipid and cholesterol synthesis (26). In APC-deficient CRC, we further document that AhR also regulates glucose uptake and overall glycolytic flux by modulating multiple glycolysis genes including SLC2A1, HK1/2, PFKL, LDHA, and ALDOA. Experimentally, TDO2 or AhR depletion resulted in downregulation of these metabolic genes and anabolic processes in APC-deficient cancer cells. In addition to metabolism, KP and AhR signaling is also known to regulate immunity in both physiological and pathological conditions. In mice, AhR plays a critical role in the maintenance and function of innate T cells in the gastrointestinal tract (27). In stress conditions, mice with whole body knockout of AhR exhibit impaired differentiation and function of T helper 17 cells and regulatory T cells to environmental toxins (28). In cancer, previous studies support both pro- and anti-tumorigenic roles for AhR. Whole body knockout of AhR in $Apc^{Min/+}$ mice causes increased cecal tumors (29), underscoring the highly context-specific actions of AhR in cancer. Further study is needed to define AhR actions in this setting which may relate to non-ligand dependent roles of AhR such as degradation of β-catenin, effects of AhR on non-cancer cell types, tissue-specific biology and/or presence of additional oncogenic mutations. In different

cancer types, regulatory mechanisms for AhR by its modulators such as ARNT, HSP90, XAP2, diverse agonists/antagonists, and direct immune modifying roles of AhR both in cancer cells and immune cells could further account for its contrasting impact on cancer. In contrast to the impact of AhR deletion in the $Apc^{Min/+}$ model, multiple reinforcing lines of evidence establish the newly identified APC-TCF4-TDO2-AhR pathway in driving cancer cell intrinsic and tumor microenvironmental processes to maintain APC-deficient CRC tumors.

With respect to translational relevance, our human CRC profiles mirrored our murine findings, showing positive correlation between TAM abundance and TDO2 expression levels. Pro-tumorigenic TAMs are known to support tumor progression and limit the efficacy of immunotherapy (30, 31). In glioblastoma, Kyn produced by glioma cells has been shown to recruit TAMs by binding to AhR and promote CD8 T cell dysfunction via expression CD39 in TAMs (32). Our TDO2 and IDO1 inhibitor study also highlights the context-specific TAM biology by the TDO2 inhibitor in APC-deficient MC38 tumors. In a recent clinical trial in melanoma targeting IDO1 with Epacadostat in combination with anti-PD1 antibody (ECHO-301), the basis for failure may relate to upregulation of IDO1 expression provoked by immune checkpoint blockade, BRAF inhibitors, or chemotherapy, resulting in inadequate target inhibition with the selected dosing of IDO1 inhibitor (33). IDO1 inhibitor studies also showed that cancer cells upregulate ABC transporters which might further reduce the availability of IDO1 inhibitor in the TME (34). Given the frequent co-expression of IDO1 and TDO2 in melanoma (19), our study also encourages the assessment of ECHO-301 post-treatment specimens which includes activation of WNT / β-catenin signaling, APC status, intratumoral Kyn

concentration, and expression of TDO2 and CXCL5. Functional redundancies between IDO1 and TDO2 may also reveal a possible compensatory mechanism involving TDO2 upregulation which would serve to sustain the Trp metabolism and KP-AhR pathway despite IDO1 inhibition. Encouragingly, however, we did not observe compensation by IDO1 upon TDO2 depletion, further underscoring the importance of understanding the common and distinct tumorigenic roles of IDO1 versus TDO2 and the genotypic context in which they operate in order to rationalize dual inhibition of IDO1/TDO2 and/or inhibition of downstream effectors such as CXCL5 (33). In conclusion, the identification of TDO2 as a synthetic essential effector of APC-deficiency in CRC may serve as a promising precision treatment for this intractable cancer.

Materials and Methods

Mice

Mice were grouped by 5 animals in large plastic cages and were maintained under pathogen-free conditions. All animal experiments were performed with the approval of MD Anderson Cancer Center's Institutional Animal Care and Use Committee (IACUC). $Apc^{Min/+}$, NSG (NOD.Cg-*Prkdc*^{scid} *Il2rg*^{tm1Wjl}/SzJ, RRID:IMSR_JAX:005557), and C57BL/6J (RRID:IMSR_JAX:000664) mice were purchased from Jackson laboratory (Stock No: 005557, 000664, 000651). Colorectal orthotopic xenograft tumor models were established following a previously published protocol (35). After orthotopic injection of cells, mice that exhibited successful tumor formation were randomized before starting Dox, antibody, or inhibitor treatment for each cell line.

iAP mice were established as described by Boutin et al. (17). Briefly, the tamoxifen-inducible Villin-Cre-ERT2 allele was crossed with the Apc Lox allele and the Tp53 Lox allele and backcrossed to C57BL/6. Cre expression driven by the Villin promoter was detected throughout the gastrointestinal tract. To limit Cre activity to the colon, we used the tamoxifen-inducible Villin-Cre-ERT2 and delivered tamoxifen directly to the colon by injecting 4-OTH into the distal colon. Sample size was determined based on previous similar experiments performed in our lab.

Cell Culture

The CRC cell lines MC38 (RRID:CVCL_B288) and its isogenic cells, as well as BMDM and HEK 293T (RRID:CVCL_0063) cells were cultured in Dulbecco's Modified Eagle's Medium (DMEM). CCD-841-CoN (ATCC Cat# CRL-1790, RRID:CVCL_2871), RKO (RRID:CVCL_0504), HT-29 (RRID:CVCL_0320), Caco-2 (RRID:CVCL_0025) and LS180 (RRID:CVCL_0397) cells were cultured in Eagle's Minimum Essential Medium (EMEM). HT-29 cells were cultured in McCoy's 5A medium. DLD-1 (RRID:CVCL_0248), CT26 (RRID:CVCL_7256), and Raw264.7 macrophage cell lines (RRID:CVCL_0493) were cultured in RPMI 1640 medium (RPMI). All cell lines were cultured in indicated medium containing 10% Tet System Approved FBS (Clontech) and 100 U/ml ampicillin/penicillin. All human cell lines have been validated through fingerprinting by the MD Anderson Cell Line Core Facility. All cells were confirmed to be mycoplasma-free and maintained at 37 °C and 5% CO_2. BMDMs from C57BL/6 mice (RRID:IMSR_JAX:000664) were cultured as previously described (36). Conditioned media were collected from treated or untreated cells as indicated after culturing for 24 h

in FBS-free culture medium. Inducible shTDO2 MC38 cell lines were treated with 1 μM of Doxycycline (Sigma-Aldrich, Cat# D9891) for indicated periods to induce TDO2 knockdown. Inhibitors and supplements used included CH223191 (Sigma-Aldrich, Cat# C8124, CAS: 301326-22-7), XAV-939 (Selleck Chemicals, Cat# S1180, CAS: 284028-89-3), recombinant mouse CXCL5 (LIX) (R&D Systems, Cat# 433-MC-025), L-Kynurenine,>=98% (HPLC) (Sigma-Aldrich, Cat# K8625).

CRISPR-Cas9 Transfection

sgRNA plasmids targeting the human APC gene (Cat# sc-400374) were purchased from Santa Cruz Biotechnology. For the mouse APC gene, a sgRNA target sequence of TTGAGCGTAGTTTCACTCCG was cloned into pCas-Guide-EF1a-GFP plasmids (Origene Technologies, Inc., Cat# GE100018). Human RKO and mouse MC38 cells were maintained in 6-well plates to 70-80% confluency in culture media supplemented with 10% heat-inactivated FBS and 100 U/ml ampicillin/penicillin. The plasmids with sgRNA were transiently transfected into cells using Lipofectamine 2000 according to the manufactory protocol. Cells were harvested 72 h later, and GFP-positive cells were sorted into each well of a 96-well plate as single cells by flow cytometry. At day 10 after cell sorting, the grown cell colonies were expanded in 24-well plates. Knock-out of the APC gene in each colony was confirmed by RT-PCR and western blot for APC and β-catenin.

Mouse Colon Organoid Culture and Genome Engineering

To isolate colonic crypts for organoid culture, a 2-cm piece of distal large intestine was incubated in PBS containing 5 mM EDTA and 0.2% FBS at 4°C for 45 min on a shaker. Incubated colon pieces were shaken vigorously to release crypts. Crypts were washed and spun down sequentially at 300 x g, 200 x g, and 100 x g to enrich for intact crypts. Crypts were resuspended in Matrigel and plated in 24-well plates containing 50 uL Matrigel per well. Organoid culture medium (500 uL) containing Wnt3a, R-spondin, Noggin, and EGF was added and changed every 2 days.

Knockout of *APC* was performed via transient transfection of a plasmid expressing Cas9 and an sgRNA targeting *APC* (*APC* sgRNA-LentiCRISPRv2; sgRNA sequence: APC-G0-1 – CGCTTGTCTAGATAAGCACG). APC-KO organoids were selected by removal of Wnt and R-spondin from the media.

Mouse $Apc^{Min/+}$ Organoids

Intestinal polyps from an 18 week-old male $Apc^{Min/+}$ mouse were harvested and the cut tissue was treated with complete chelating solution containing 30 mM EDTA for 30 min at 4ºC. The tissue pieces were then pipetted gently to dissociate the crypts. These crypts were then seeded in Matrigel (Corning, Cat# 47743-722) in the presence of high WNT organoid media in the presence of ROCK inhibitor Y-27632 (STEMCELL Technologies Inc., Cat# 72302) for 7-10 days.

Human Samples

Human CRC tissue microarray (TMA) slides were obtained from the Department of Pathology at the University of Texas MD Anderson Cancer Center. Studies related to

human specimens were approved by the MD Anderson Institutional Review Board under protocol Lab09-0373.

Mutual exclusivity analysis

For the analysis of mutual exclusiveness for APC in colorectal cancer, genetic alteration data of 220 TCGA CRC samples with copy number alterations and sequencing data were downloaded from cBioPortal (RRID:SCR_014555); the gene expression dataset was downloaded from the Broad GDAC website (http://gdac.broadinstitute.org/runs/stddata__2016_01_28/data/COAD/20160128/); The detailed method for estimating mutation exclusivity was previously described (*8*). Briefly, the rank score (odds ratio score) was calculated to indicate mutual exclusiveness between gene A and gene B deletion. The mean values of gene B expression in all 220 samples and that in gene A deleted samples were calculated and analyzed with Student's t-test. For *APC* mutations in CRC datasets, only deletion and mutations with known significance (annotated by OncoKB, RRID:SCR_014782) cases were considered. The list of mutual exclusive genes to APC are listed in Table S1.

TCGA data computational analysis

For analysis of human CRC and BRCA data, we downloaded the gene expression and copy number data of TCGA datasets or other available datasets from cBioPortal (RRID:SCR_014555). Correlation analysis of TDO2, AhR, and CYP1B1 expression in CRC was performed with R2 platform: https://r2.amc.nl/.

Gene stable shRNA/siRNA knockdown and inducible shRNA knockdown

Mission shRNA hairpins targeting mouse TDO, AhR, and TCF4 were purchased from Santa Cruz; GIPZ shRNA hairpins targeting human TDO were purchased from Horizon Discovery. For inducible TDO2 knockdown, SMARTvector Inducible Lentiviral shRNA for mouse TDO2 was purchased from Horizon Discovery. The sequences that reduced mRNA and/or protein levels by >70% were chosen. For in vivo bioluminescence imaging, luciferase vector EF1-RFP-T2A-Luciferase (system Biosciences, Cat# BLIV502MC-1) and D-Luciferin (Perkin Elmer, Cat# NC0921725) were used. Recombinant lentiviral particles were produced by transient transfection of plasmids into HEK293T cells (RRID:CVCL_0063). In brief, 8 μg of shRNA plasmid, 4 μg of psPAX2 plasmid (RRID:Addgene_12260), and 2 μg of pMD2.G plasmid (RRID:Addgene_12259) were transfected using Lipofectamine 3000 into 293T cells plated in 100-mm dishes. Viral supernatant was collected 48 h and 72 h after transfection and filtered. Cells were infected twice in 48 h with viral supernatant containing 8 μg/ml polybrene, and then selected using 2 μg/ml puromycin. Expression of TDO2, AhR, and TCF4 were measured by RT-qPCR. The following shRNA sequences were used.

Human shTDO2 #3: NM_005651: 5'-AATCTGATTCATCACTGCT-3',

Human shTDO2 #6: NM_005651: 5'-AAATCTACAAATACCTTGT-3',

Mouse shTDO2 #2: NM_019911: 5'-CGGCCAAAGATGAATCCGATCATTCTCGAGA ATGATCGGATTCATCTTTGGTTTTTG-3',

Mouse shTDO2 #4: NM_019911: 5'-GGGCGCAAGAACTTCAGAGTGAACTCGAGTTCACTCTGAAGTTCTTGCGCTTTTTG-3',

Mouse ishTDO2 #3: NM_019911.2: 5'-GGATTTAATTTCTGGGGAA-3',

Mouse shAhR #1: NM_013464: 5'-CGGCATCGACATAACGGACGAAATCTCGAGATTTCGTCCGTTATGTCGATGTTTTTG-3',

Mouse shAhR #2: NM_013464: 5'-GTACCGGGTCAAGCCTGTTAGCTATATTCTCGAGAATATAGCTAACAGGCTTGACTTTTTTG-3',

Human shTCF4 #1: NM_030756: 5'-CCGGCCTTTCACTTCCTCCGATTACCTCGAGGTAATCGGAGGAAGTGAAAGGTTTTTG -3',

Human shTCF4 #2: NM_030756: 5'-CCGGAGAGAAGAGCAAGCGAAATACCTCGAGGTATTTCGCTTGCTCTTCTCTTTTTTG -3',

For siRNA experiments, Lipofectamine RNAiMAX Transfection Reagent (Thermo Fisher, Cat# 13778030) was used and the assay performed following manufacturer's protocol. Transfected cells were maintained for three days and knockdown efficiency for TCF4 was measured by western blotting. The following siRNAs (Sigma-Aldrich) were used.

Human siTCF4 #1: NM_030756: SASI_Hs01_00197690

Human siTCF4 #2: NM_030756: SASI_Hs01_00197691

Human siTCF4 #3: NM_030756: SASI_Hs01_00197692

Mouse siTCF4 #1: NM_009333: SASI_Mm01_00142189

Mouse siTCF4 #2: NM_009333: SASI_Mm02_00315891

Mouse siTCF4 #3: NM_009333: SASI_Mm01_00142190

Western blot

Cell lysates were prepared with RIPA lysis buffer (Roche) with Halt™ Protease and Phosphatase Inhibitor Single-Use Cocktail (Thermo, 78442). Immunoblotting was performed following standard protocol. Antibodies were purchased from the indicated companies: β-actin (Sigma-Aldrich, Cat# A1978, RRID:AB_476692), APC (Santa Cruz Biotechnology, Cat# sc-896, RRID:AB_2057493), tubulin (Sigma-Aldrich, Cat#T9026; RRID: AB_477593), vinculin (Millipore, Cat# 05-386, RRID:AB_309711), TDO2 (Origene, Cat# TA504730, RRID:AB_2622554), β-catenin (Cell signaling Technology, Cat# 9587, RRID:AB_10695312), TCF4 (Santa Cruz Biotechnology, Cat# sc-166699, RRID:AB_2199823), phospho-eIF2 (Cell Signaling Technology Cat# 9721, RRID:AB_330951), eIF2 (Cell Signaling Technology Cat# 9722, RRID:AB_2230924), ATF4 (Cell Signaling Technology Cat# 11815, RRID:AB_2616025), phospho-mTOR (Cell Signaling Technology Cat# 2971, RRID:AB_330970), mTOR (Cell Signaling Technology Cat# 2972, RRID:AB_330978), GCN2 (Santa Cruz Biotechnology Cat# sc-374609, RRID:AB_10986130), and cleaved Caspase-3 (Cell signaling Technology, Cat# 9661, RRID:AB_2341188).

ORF and hairpin-resistant ORF expression

To construct hairpin-resistant hTDO2 ORF expression vector to shTDO2 #3, site-directed mutagenesis was performed on human TDO2 ORF gene in pcDNA3.1+/C-(k)DYK vector (GenScript, Cat# OHu09674D). Nucleotide mutation was targeted for 1) 1272 T to C, 2)1275 T to C, 3) 1278 A to G, 4) 1281 A to G and no amino acid was altered. Mutated TDO2 ORF gene insert was subcloned into PS100102 (pLenti-C-mGFP-P2A-BSD Tagged Cloning Vector; Origene, Cat# PS10094).

For mutagenesis, following primers were used:

F: 5'-CCTACTTCAGCAGCGACGAGTCGGATTAAAATCG-3'

R: 5'-CGATTTTAATCCGACTCGTCGCTGCTGAAGTAGG-3'

Lentiviral ORF expressing vectors for blank, CXCL5, CXCL7, and CSF3 were purchased from ABM (Cat# LV587, LV407122, LV395200, LV455866).

For Seahorse glycolytic flux assay in TDO2 overexpressing cells, mouse TDO2 ORF (NM_019911) expressing vector was purchased from GenScript (Cat# OMu17612D).

Luciferase assay

HEK 293T cells were seeded in 24-well plates and transfected with luciferase reporter vectors of pGL3-Basic (Promega, Cat# E1751), pGL3-hTDO2 promoter, or pGL3-hTDO2 promoter with a mutated TCF4 binding site with pRL Renilla Luciferase Control Reporter Vector (Promega, Cat# E2261) and pLV-beta-catenin ΔN90 (RRID:Addgene_36985) using Lipofectamine 2000 reagent (Thermo, Cat# 11668019). pcDNA/Myc DeltaN TCF4 expression vector (RRID:Addgene_16513) was transfected to

express dominant negative TCF4. Luciferase activity was measured with Dual-Luciferase reagent (Promega, E1910) according to the manufacturer's instructions.

Glycolytic flux measurement

Agilent Seahorse XF Glycolysis stress test kit (Agilent Cat# 103020-100) was used to measure glycolytic flux according to the manufacturer's instructions. In brief, MC38 cells expressing Blank-ORF or TDO2-ORF 96-well XF were plated at 2×10^4 cells per wells in 96-well Seahorse plate in DMEM and were incubated overnight. The next day, culture medium was removed and changed with Seahorse XF DMEM assay medium (Agilent Cat# 103680-100) containing 2 mM L-glutamine. Cells were incubated in the assay medium for 1 hr and sensor cartridges incubated in calibrant solution (Agilent Cat# 100840-000) were loaded with glucose, oligomycin and 2-DG (Final working concentrations: 1 mM glucose, 1μM oligomycin and 50 mM 2—DG). Glycolytic flux was measured using an Agilent Seahorse XF^e Analyzer (Agilent Technologies). Raw data were analyzed with Wave software (Agilent Technologies).

Cytokine array

For cytokine array, CRC orthotopic tumors established with ishTDO2 APC-WT and APC-KO MC38 cells were incubated in RIPA buffer with protease/phosphatase inhibitor cocktail and homogenized. Cytokine array was performed with mCytokine Array Kit, Panel A (R&D Systems, Cat# ARY006) following the manufacturer's protocol. For phospho-RTK array, ishTDO2 APC-WT and APC-KO MC38 cells were treated with dox for 48 hr and the lysates were used for the array.

667

668 **Immunohistochemistry and immunofluorescence**

669 Immunohistochemistry was performed using a standard protocol we previously
670 described (37). Antibodies were: TDO2 (Abnova Corporation, Cat# H00006999-B01P,
671 RRID:AB_1138993), AhR (Santa Cruz Biotechnology, Cat#sc-133088,
672 RRID:AB_2273721), β-catenin (Cell signaling Technology, Cat# 9587,
673 RRID:AB_10695312), Ki67 (Thermo Fisher Scientific, Cat# MA1-90584,
674 RRID:AB_2314700), Cleaved caspase-3 (Cell signaling Technology, Cat# 9661,
675 RRID:AB_2341188), F4/80 (Cell signaling Technology, Cat# 70076,
676 RRID:AB_2799771), CD163 (abcam, Cat# ab182422, RRID:AB_2753196), CD206
677 (BioLegend, Cat#141705, RRID:AB_10896421). For immunofluorescence staining, CD8
678 (Cell signaling Technology, Cat# 98941, RRID:AB_2756376) and Granzyme B (Thermo
679 Fisher Scientific, Cat# MA1-80734, RRID:AB_931084) antibodies were used. For nuclei
680 staining, DAPI (Thermo Fisher Scientific Cat# D1306, RRID:AB_2629482) was used.
681 The human and mouse tumor tissue sections were reviewed and scored.

682

683 **Migration assay**

684 Macrophages (1×10^4 for Raw264.7 and BMDM) were suspended in serum-free
685 culture medium and seeded into 24-well Transwell inserts (5.0 μm, Corning, Cat#
686 CLS3422). Medium with indicated factors or conditioned media was added to the
687 remaining receiver wells. The CXCR1/2 inhibitor SX-682 was obtained from Syntrix
688 Biosystems. After 24 h, the migrated macrophages were fixed and stained with crystal
689 violet (0.05%, sigma), and counted with ImageJ (RRID:SCR_003070).

690

691 **Colony formation assay**

692 Colorectal cancer cell proliferation in vitro was assayed through colony formation.
693 Cells (1×10^3) were seeded in 6-well plates and cultured for 5-7 days and then fixed
694 and stained with 0.5% crystal violet in 25% methanol for 1 hr. These experiments were
695 performed in triplicate.

696

697 **In vivo TDO2 inhibitor drug treatment**

698 For C57BL/6J mice with APC-WT and APC-KO MC38 tumors, TDO2 inhibitor (200
699 mg/kg, synthesized in house) was dissolved in 0.5% HPMC before each injection and
700 administrated orally twice daily by oral gavage. Epacadostat (Medchemexpress, Cat#
701 HY-15689) was dissolved in 10% DMSO and further diluted in 90% corn oil and
702 administrated twice daily at 100 mg/kg by oral gavage.

703 For iAP mice, APC and TP53 deletions were induced by injecting 4-OHT into distal
704 colon. Three weeks after induction, 0.5% HPMC or TDO2 inhibitor (100 mg/kg) was
705 administered daily by oral gavage to randomized mice.

706

707 **In vivo neutralizing antibody treatment and macrophage depletion**

708 For CXCL5 neutralizing experiment, Rat IgG2b Isotype Control (Cat# BE0090)
709 was purchased from BioXCell; anti-Mouse CXCL5 (Clone 61905) neutralizing antibody
710 was purchased from Leinco Technologies (Cat# C1414). For macrophage depletion
711 study, Standard Macrophage Depletion Kit (Clodrosome + Encapsome) (Encapsula
712 NanoSciences, Cat# CLD-8901) was used following manufacture's protocol.

Mass Cytometry (CyTOF)

CyTOF analysis was performed as described previously (37). Briefly, tumors were digested and single cells blocked with FcR were incubated with surface antibody. Cells were then incubated with Cell-ID Cisplatin (Fluidigm, Cat# 201064) and permeabilized for FOXP3 intracellular staining. For nuclei staining, cells were incubated with Cell-ID Intercalator-Ir (Fluidigm, Cat #201192A) during fixing. Samples were analyzed with a CyTOF instrument (Fluidigm) in the Flow Cytometry and Cellular Imaging Core Facility at MD Anderson Cancer Center. Cell numbers and percentages of each cell population were analyzed with FlowJo (Tree Star, RRID:SCR_008520) and GraphPad Prism 6 software (RRID:SCR_002798). CyTOF data were visualized using a dimensionality reduction method viSNE (38), which was implemented using the Cytobank (RRID:SCR_014043) (39).

Kyn, 2-DG uptake and lactate secretion measurement

Kyn concentration was measured following manufacturer's protocol for Kyn ELISA measurement kit (ImmuSmol, Cat# BA-E-2200). The 2-DG uptake assay was performed according to manufacturer's protocol for 2-Deoxyglucose Uptake measurement kit (Cosmo Bio, Cat# CSR-OKP-PMG-K01TE). For secreted lactate measurement, Lactate Colorimetric/Fluorometric Assay Kit (BioVision, Cat# 10186-852) was used and assay was performed following manufacturer's protocol.

LC-MS/MS-Based Targeted Metabolomics

Media from cultured cells were harvested and quickly placed into dry ice or -80°C freezer. Cells were washed twice with ice-cold PBS and snap-frozen using liquid nitrogen. Frozen cells were scraped into 1 mL of -70°C-cooled 80% methanol and quickly stored at -80°C. LC-MS/MS analyses were performed on an AB SCIEX QTRAP 6500 LC-MS/MS system by the Karmanos Cancer Institute Pharmacology Core. Analyst 1.6 software was used for system control and data acquisition, and MultiQuant 3.0 software was used for data processing and quantitation. For statistical analysis, Metaboanalyst (RRID:SCR_015539) was used.

ChIP–sequencing and ChIP-PCR

ChIP was performed as we described recently (9). Briefly, chromatin from PFA-fixed cells were cross-linked with 1% PFA and then reactions were quenched using 0.125 M glycine. Cells were lysed with ChIP lysis buffer [10 mM Tris-HCl (pH 8.0), 140 mM NaCl, 1 mM EDTA (pH 8.0), 1% Triton X-100, 0.2% SDS and 0.1% deoxycholic acid] for 30 min on ice. Chromatin fragmentation was performed using a Diagenode BioruptorPico sonicator (30 s on and 30 s off, 45 cycles) and incubated with the appropriate mixture of antibody and Dynabeads (ThermoFisher Scientific, Cat# 10003D) overnight. Immune complexes were washed with RIPA buffer (three times), once with RIPA-500 (RIPA with 500 mM NaCl), and once with LiCl wash buffer [10 mM Tris-HCl (pH 8.0), 1 mM EDTA (pH 8.0), 250 mM LiCl, 0.5% NP-40 and 0.5% deoxycholic acid]. Elution and reverse-crosslinking were performed in direct elution buffer [10 mM Tris-Cl (pH 8.0), 5 mM EDTA, 300 mM NaCl, 0.5% SDS] containing proteinase K (20 mg/ml) at 65°C overnight. Eluted DNA was purified using AMPure beads (Beckman-Coulter, Cat#

A63880), and then used to generate libraries using NEBNext Ultra DNA Library kit (New England BioLabs Inc., Cat# E7370), or to perform qPCR. Sequencing was performed using an Illumina HiSeq 2500 instrument to generate dataset. CHIP-PCR primers are following:

hGAPDH promoter F: ACTGAGCAAGAGAGGCCCTA-

R: TATGGGGGTCTGGGATGGAA-

hAxin2 promoter F: CTCGCATACCTCCCTTCC-

R: TTCCAGCAGTCACTAGGC-

hc-Myc promoter F: CTCACTGGAACTTACAATCTG-

R: CAACGCCCAAAGGAAATC-

hTDO2 Promoter. F: GCATGCTGATTGGCTGATGC-

R: AAAACAACCCAGATGTTCTACAGC-

mRNA expression analysis, microarray and RNA sequencing

Cells were pelleted and RNA was isolated with RNeasy Mini Kit (Qiagen, Cat# 74104). RNA was reverse-transcribed into cDNA following SuperScript™ III First-Strand Synthesis SuperMix (Invitrogen, Cat# 18080400). qRT-PCR was performed using SYBR Green PCR Master Mix (Thermo Fisher Scientific) in a 7500 Fast Real-Time PCR instrument (Applied Biosystems). qRT-PCR primers are following; hAPC;F: TCTTGGCGAGCAGATGTAAA- R: TCCACAAAGTTCCACATGC-, hTDO2;F: GGGAACTACCTGCATTTGGA- R: GTGCATCCGAGAAACAACCT-, hAhR;F: ATTGTGCCGAGTCCCATATC- R: AAGCAGGCGTGCATTAGACT-, hCyp1A1;F: CTTGGACCTCTTTGGAGCT- R: GACCTGCCAATCACTGTG-, hCyp1B1;F:

GACGCCTTTATCCTCTCTGCG- R: ACGACCTGATCCAATTCTGCC-, hGAPDH;F: GTCTCCTCTGACTTCAACAGCG- R: ACCACCCTGTTGCTGTAGCCAA-, mAPC;F: CTTGTGGCCCAGTTAAAATCTGA- R: CGCTTTTGAGGGTTGATTCCT-, mTDO2;F: ATGAGTGGGTGCCCGTTTG- R: GGCTCTGTTTACACCAGTTTGAG-, mAhR;F: AGCCGGTGCAGAAAACAGTAA- R: AGGCGGTCTAACTCTGTGTTC-, mCyp1A1;F: GACACAGTGATTGGCAGAG- R: GAAGGTCTCCAGAATGAAGG-, mCyp1B1;F: CACCAGCCTTAGTGCAGACAG-R: GAGGACCACGGTTTCCGTTG-, mHK1;F: CGGAATGGGGAGCCTTTGG- R: GCCTTCCTTATCCGTTTCAATGG-, mHK2;F: TGATCGCCTGCTTATTCACGG- R: AACCGCCTAGAAATCTCCAGA-, mSLC2A1;F: GCAGTTCGGCTATAACACTGG- R: GCGGTGGTTCCATGTTTGATTG-, mPFKL;F: GGAGGCGAGAACATCAAGCC- R: CGGCCTTCCCTCGTAGTGA-, mLDHA;F: GCTCCCCAGAACAAGATTACAG- R: TCGCCCTTGAGTTTGTCTTC-, mALDOA;F: CGTGTGAATCCCTGCATTGG- R: CAGCCCCTGGGTAGTTGTC-, mCXCL5;F: TCCAGCTCGCCATTCATGC- R: TTGCGGCTATGACTGAGGAAG-, mCXCL7;F: CTCAGACCTACATCGTCCTGC- R: GTGGCTATCACTTCCACATCAG-, mCSF3;F: ATGGCTCAACTTTCTGCCCAG- R: CTGACAGTGACCAGGGGAAC-, mCXCR2;F: ATGCCCTCTATTCTGCCAGAT- R: GTGCTCCGGTTGTATAAGATGAC-, mCSF1; F: ATGAGCAGGAGTATTGCCAAGG- R: TCCATTCCCAATCATGTGGCTA-, mCD206;F: CTCTGTTCAGCTATTGGACGC- R: CGGAATTTCTGGGATTCAGCTTC-, mYM1;F: CAGGTCTGGCAATTCTTCTGAA- R: GTCTTGCTCATGTGTGTAAGTGA-, mYM2;F: TCCACTTTGAACCACATTCCAA- R: CCAGCACTAACAGTAGGGTCA-, mArg1;F: CTCCAAGCCAAAGTCCTTAGAG- R:

AGGAGCTGTCATTAGGGACATC-, miNOS;F: GTTCTCAGCCCAACAATACAAGA-R: GTGGACGGGTCGATGTCAC-, mbeta-actin;F: AAATCTGGCACCACACCTTC- R: GGGGTGTTGAAGGTCTCAAA-, mGAPDH;F: GCCTTCCGTGTTCCTACCC- R: CAGTGGGCCCTCAGATGC-

The expression of each gene was normalized to that of GAPDH or Actin. For microarray, tumors established with ishTDO2 APC-WT and APC-KO MC38 cells were harvested (biological triplicates for control and APC-KO MC38 tumors). RNAs were isolated using Trizol (Invitrogen, Cat# 15596-026) and further purified with the RNeasy Mini Kit. Samples were analyzed at the MD Anderson Microarray Core facility using the GeneChip Mouse Clariom D array (Affymetrix) to generate dataset. Genes that were differentially expressed between control and APC-depleted MC38 cells were subjected to gene set enrichment analysis (GSEA). For RNA sequencing, RNAs were isolated from ishTDO2 APC-WT and APC-KO MC38 cells with and without Dox treatment (biological triplicates per group) using the RNeasy Mini Kit. Illumina TrueSeq CHIP library was used for Illumina Next Seq 500 Sequencing.

Tumor-infiltrated macrophage RNA isolation and sequencing

Tumor infiltrated macrophage isolation and sorting from MC38 tumors were performed by following a published protocol (40) with slight modifications. Briefly, APC-WT and APC-KO MC38 tumors (two per group) implanted in C57BL/6J mice were digested with Liberase DL (Roche) and Liberase TL. After RBC lysis, cells were blocked with CD16/CD32 blocking antibody (BD Biosciences Cat# 553142, RRID:AB_394657)

for 30 min and stained with antibodies: CD45 APC 30-F11 (BD Biosciences Cat# 553142, RRID:AB_394657) for 30 min and stained with antibodies: CD45 APC 30-F11 (BioLegend Cat# 103111, RRID:AB_312976), CD11b eFluor 605 M1/70 (Thermo Fisher Scientific Cat# 69-0112-82, RRID:AB_2637406), F4/80 PerCp-Cy5.5 BM8 (BioLegend Cat# 123127, RRID:AB_893496), CD206/MMR 169tm C068C2 (Fluidgm Cat# 3169021B, RRID:AB_2832249) and SYTOX green (ThermoFisher Cat# R37168). Stained cells were sorted as CD45+, CD11b+, F4/80+ and CD206+. Total RNA was isolated from sorted cells and were sequenced by Ultra low Input RAN sequencing (Illumina NexteraXT) with six replicates of each sample. Comparisons between groups were hampered by low input of total RNA isolated from tumor macrophages manifesting as inconsistent raw/normalized read counts for housekeeping genes in the different groups. To enable comparisons between APC-WT and APC-KO tumors, we re-normalized the read counts of multiple M2 macrophage markers with housekeeping gene read counts (GAPDH and ACTB) (41).

Quantification and statistical analysis

The analysis of TAM IHC staining for correlation with nuclear β-catenin, TDO2, and CD163 was performed using the chi-squared test. Mouse survival analysis was performed using Log-rank (Mantel-Cox) test (GraphPad Prism 9, RRID:SCR_002798). All other statistical analyses were performed with Student's t-test and represented as mean ± SD. The p values were designated as: *, $p<0.05$; **, $p<0.01$; and ***, $p<0.001$; n.s. non-significant ($p>0.05$).

Data Availability

RNA-seq, ChIP-seq, and microarray data have been deposited in the NCBI GEO with the accession numbers GSE200910, GSE201414, and GSE201415, respectively. Additional data, reagents, and materials generated in this study can be obtained from the corresponding authors upon request.

Acknowledgments

This study is dedicated to the memory of Alvaro DePinho who succumbed to CRC and continues to serve as an inspiration to R.A.D. The authors thank Dr. Scott Kopetz, Dr. Guillermina Lozano, and Dr. Trevor Hart for scientific discussion and advice; Dr. Dipen Maru for human CRC TMA samples; Institute for Applied Cancer Science (IACS) for inhibitor synthesis and distribution; Dr. Jing Li for metabolomics analysis. The results shown here are in whole or part based upon data generated by the TCGA Research Network: https://www.cancer.gov/tcga.

References

1. Vogelstein B, Papadopoulos N, Velculescu VE, Zhou S, Diaz LA, Jr., Kinzler KW. Cancer genome landscapes. Science. 2013;339(6127):1546-58.

2. Su LK, Kinzler KW, Vogelstein B, Preisinger AC, Moser AR, Luongo C, et al. Multiple intestinal neoplasia caused by a mutation in the murine homolog of the APC gene. Science. 1992;256(5057):668-70.

874 3. Dow LE, O'Rourke KP, Simon J, Tschaharganeh DF, van Es JH, Clevers H, et al.
875 Apc Restoration Promotes Cellular Differentiation and Reestablishes Crypt
876 Homeostasis in Colorectal Cancer. Cell. 2015;161(7):1539-52.
877 4. Fang DC, Luo YH, Yang SM, Li XA, Ling XL, Fang L. Mutation analysis of APC
878 gene in gastric cancer with microsatellite instability. World J Gastroenterol.
879 2002;8(5):787-91.
880 5. Furuuchi K, Tada M, Yamada H, Kataoka A, Furuuchi N, Hamada J, et al.
881 Somatic mutations of the APC gene in primary breast cancers. Am J Pathol.
882 2000;156(6):1997-2005.
883 6. Horii A, Nakatsuru S, Miyoshi Y, Ichii S, Nagase H, Ando H, et al. Frequent
884 somatic mutations of the APC gene in human pancreatic cancer. Cancer Res.
885 1992;52(23):6696-8.
886 7. Ohgaki H, Kros JM, Okamoto Y, Gaspert A, Huang H, Kurrer MO. APC mutations
887 are infrequent but present in human lung cancer. Cancer Lett. 2004;207(2):197-203.
888 8. MacDonald BT, Tamai K, He X. Wnt/beta-catenin signaling: components,
889 mechanisms, and diseases. Dev Cell. 2009;17(1):9-26.
890 9. Zhao D, Lu X, Wang G, Lan Z, Liao W, Li J, et al. Synthetic essentiality of
891 chromatin remodelling factor CHD1 in PTEN-deficient cancer. Nature.
892 2017;542(7642):484-8.
893 10. Zhao D, DePinho RA. Synthetic essentiality: Targeting tumor suppressor
894 deficiencies in cancer. Bioessays. 2017;39(8).
895 11. Hu C, Pang B, Lin G, Zhen Y, Yi H. Energy metabolism manipulates the fate and
896 function of tumour myeloid-derived suppressor cells. Br J Cancer. 2020;122(1):23-9.

12. D'Amato NC, Rogers TJ, Gordon MA, Greene LI, Cochrane DR, Spoelstra NS, et al. A TDO2-AhR signaling axis facilitates anoikis resistance and metastasis in triple-negative breast cancer. Cancer Res. 2015;75(21):4651-64.

13. Opitz CA, Litzenburger UM, Sahm F, Ott M, Tritschler I, Trump S, et al. An endogenous tumour-promoting ligand of the human aryl hydrocarbon receptor. Nature. 2011;478(7368):197-203.

14. Rosenbluh J, Nijhawan D, Cox AG, Li X, Neal JT, Schafer EJ, et al. beta-Catenin-driven cancers require a YAP1 transcriptional complex for survival and tumorigenesis. Cell. 2012;151(7):1457-73.

15. Van der Flier LG, Sabates-Bellver J, Oving I, Haegebarth A, De Palo M, Anti M, et al. The Intestinal Wnt/TCF Signature. Gastroenterology. 2007;132(2):628-32.

16. Subramanian A, Tamayo P, Mootha VK, Mukherjee S, Ebert BL, Gillette MA, et al. Gene set enrichment analysis: a knowledge-based approach for interpreting genome-wide expression profiles. Proc Natl Acad Sci U S A. 2005;102(43):15545-50.

17. Boutin AT, Liao WT, Wang M, Hwang SS, Karpinets TV, Cheung H, et al. Oncogenic Kras drives invasion and maintains metastases in colorectal cancer. Genes Dev. 2017;31(4):370-82.

18. Pilotte L, Larrieu P, Stroobant V, Colau D, Dolusic E, Frederick R, et al. Reversal of tumoral immune resistance by inhibition of tryptophan 2,3-dioxygenase. Proc Natl Acad Sci U S A. 2012;109(7):2497-502.

19. Muller AJ, Manfredi MG, Zakharia Y, Prendergast GC. Inhibiting IDO pathways to treat cancer: lessons from the ECHO-301 trial and beyond. Semin Immunopathol. 2019;41(1):41-8.

20. Schramme F, Crosignani S, Frederix K, Hoffmann D, Pilotte L, Stroobant V, et al. Inhibition of Tryptophan-Dioxygenase Activity Increases the Antitumor Efficacy of Immune Checkpoint Inhibitors. Cancer Immunol Res. 2020;8(1):32-45.

21. Pate KT, Stringari C, Sprowl-Tanio S, Wang K, TeSlaa T, Hoverter NP, et al. Wnt signaling directs a metabolic program of glycolysis and angiogenesis in colon cancer. EMBO J. 2014;33(13):1454-73.

22. van Baren N, Van den Eynde BJ. Tryptophan-degrading enzymes in tumoral immune resistance. Front Immunol. 2015;6:34.

23. Ott M, Litzenburger UM, Rauschenbach KJ, Bunse L, Ochs K, Sahm F, et al. Suppression of TDO-mediated tryptophan catabolism in glioblastoma cells by a steroid-responsive FKBP52-dependent pathway. Glia. 2015;63(1):78-90.

24. Puccetti P. On the Non-Redundant Roles of TDO2 and IDO1. Front Immunol. 2014;5:522.

25. Badawy AA. Kynurenine Pathway of Tryptophan Metabolism: Regulatory and Functional Aspects. Int J Tryptophan Res. 2017;10:1178646917691938.

26. Gabriely G, Wheeler MA, Takenaka MC, Quintana FJ. Role of AHR and HIF-1alpha in Glioblastoma Metabolism. Trends Endocrinol Metab. 2017;28(6):428-36.

27. Stange J, Veldhoen M. The aryl hydrocarbon receptor in innate T cell immunity. Semin Immunopathol. 2013;35(6):645-55.

28. Quintana FJ, Basso AS, Iglesias AH, Korn T, Farez MF, Bettelli E, et al. Control of T(reg) and T(H)17 cell differentiation by the aryl hydrocarbon receptor. Nature. 2008;453(7191):65-71.

942 29. Kawajiri K, Kobayashi Y, Ohtake F, Ikuta T, Matsushima Y, Mimura J, et al. Aryl
943 hydrocarbon receptor suppresses intestinal carcinogenesis in ApcMin/+ mice with
944 natural ligands. Proc Natl Acad Sci U S A. 2009;106(32):13481-6.
945 30. Liu Y, Cao X. The origin and function of tumor-associated macrophages. Cell Mol
946 Immunol. 2015;12(1):1-4.
947 31. Pathria P, Louis TL, Varner JA. Targeting Tumor-Associated Macrophages in
948 Cancer. Trends Immunol. 2019;40(4):310-27.
949 32. Takenaka MC, Gabriely G, Rothhammer V, Mascanfroni ID, Wheeler MA, Chao
950 CC, et al. Control of tumor-associated macrophages and T cells in glioblastoma via
951 AHR and CD39. Nat Neurosci. 2019;22(5):729-40.
952 33. Opitz CA, Somarribas Patterson LF, Mohapatra SR, Dewi DL, Sadik A, Platten M,
953 et al. The therapeutic potential of targeting tryptophan catabolism in cancer. Br J Cancer.
954 2020;122(1):30-44.
955 34. Zhang Q, Zhang Y, Boer J, Shi JG, Hu P, Diamond S, et al. In Vitro Interactions
956 of Epacadostat and its Major Metabolites with Human Efflux and Uptake Transporters:
957 Implications for Pharmacokinetics and Drug Interactions. Drug Metab Dispos.
958 2017;45(6):612-23.
959 35. Tseng W, Leong X, Engleman E. Orthotopic mouse model of colorectal cancer. J
960 Vis Exp. 2007(10):484.
961 36. Chen P, Zhao D, Li J, Liang X, Li J, Chang A, et al. Symbiotic Macrophage-
962 Glioma Cell Interactions Reveal Synthetic Lethality in PTEN-Null Glioma. Cancer Cell.
963 2019;35(6):868-84 e6.

964 37. Liao W, Overman MJ, Boutin AT, Shang X, Zhao D, Dey P, et al. KRAS-IRF2
965 Axis Drives Immune Suppression and Immune Therapy Resistance in Colorectal
966 Cancer. Cancer Cell. 2019;35(4):559-72 e7.
967 38. Amir ED, Davis KL, Tadmor MD, Simonds EF, Levine JH, Bendall SC, et al.
968 viSNE enables visualization of high dimensional single-cell data and reveals phenotypic
969 heterogeneity of leukemia. Nature Biotechnology. 2013;31(6):545-+.
970 39. Chen TJ, Kotecha N. Cytobank: providing an analytics platform for community
971 cytometry data analysis and collaboration. Curr Top Microbiol Immunol. 2014;377:127-
972 57.
973 40. Cassetta L, Noy R, Swierczak A, Sugano G, Smith H, Wiechmann L, et al.
974 Isolation of Mouse and Human Tumor-Associated Macrophages. Adv Exp Med Biol.
975 2016;899:211-29.
976 41. Abrams ZB, Johnson TS, Huang K, Payne PRO, Coombes K. A protocol to
977 evaluate RNA sequencing normalization methods. BMC Bioinformatics. 2019;20(Suppl
978 24):679.
979
980
981 **Author contributions**
982 R.L. and R.A.D. conceptualized the project, designed the experiments, interpreted the
983 results, and wrote the manuscript. J.L. analyzed CHIP sequencing data. J.L. and C.W.
984 performed genomic dataset sample clustering and gene expression analysis. Jun Li
985 performed mutual exclusivity analysis. S.J. assisted with animal experiments. K.A.L
986 generated and provided APC-intact and APC-null mouse colon organoids. D.C., P.C.,

Y.A.W., and D.Z interpreted the data. D.S. helped edit the manuscript and reviewed data.

Figure Legends

Fig. 1. TDO2 as a synthetic essential gene for mutant *APC* gene in CRC. (A) Venn diagram analysis using three different datasets identified TDO2 as a top potential SE gene. **(B)** TDO2 mRNA expression is significantly correlated with expression of WNT pathway signature genes in TCGA CRC (COAD + READ, Provisional) patients (n=433). ****P<0.0001. **(C)** Representative images of IHC staining for TDO2 in serial sectioned human CRC tumors with negative (n=34) and positive nuclear β-catenin (n=47). Scale bars, ×10 (200 μm) and ×40 (50 μm). **(D)** CRC tumors with nuclear β-catenin showed higher TDO2 expression (TDO2 staining score 0-3). Pearson Correlation Coefficient =42.342, ****P<0.0001. Chi-squared test. **(E)** IHC analysis of CRC tumors from iAP and iKAP mice showed increased nuclear β-catenin, Ki67, and TDO2 compared to normal colon tissue. Scale bar, 100 μm for iAP and 500 μm for iKAP. **(F)** Immunoblotting for TDO2 in organoids isolated from C57BL/6J ileum and $Apc^{Min/+}$ mice. **(G)** Immunoblotting for TDO2 in colonoids isolated from C57BL/6J mice. APC-KO colonoids were APC-deleted by CRISPR-Cas9.

Fig. 2. TCF4/TCF7L2 mediates upregulation of TDO2 in APC-mutated CRC cells. (A) Immunoblots for TDO2 and β-catenin in CRC cell lines RKO (human) and MC38

(mouse) with their isogenic APC-KO counterparts. At least three independent experiments were performed. **(B)** RT-qPCR shows APC-deleted RKO and MC38 cell lines exhibit increased TDO2 mRNA expression. At least three independent experiments were performed. *P<0.05, **P<0.01, ****P<0.0001. **(C)** DNA sequence binding motif for transcription factor TCF4/TCF7L2. Promoter regions of human and mouse TDO2 genes harbor TCF4 binding motifs near transcription start site. The motif sequence is conserved in human and mouse genes. **(D)** ChIP-seq in APC-WT and APC-KO MC38 cells showed binding peaks for TCF4 on the promoters of TDO2 gene. **(E)** ChIP-PCR using TCF4 antibody showed enriched binding to the promoter regions of TDO2 gene in DLD-1 cells. GAPDH as negative control; MYC and AXIN2 as positive controls. **(F)** Luciferase activity of hTDO2 promoter in HEK 293T cells with constitutively active form of β-catenin (Δ90) when co-transfected with dominant negative (DN) TCF4. ***P<0.001. Two independent experiments were performed. **(G)** Luciferase activity of hTDO2 promoter in HEK 293T cells with constitutively active form of β-catenin (Δ90) and dominant negative (DN) TCF4. **P<0.01. **(H)** Luciferase activity of TCF4 binding motif-mutated hTDO2 promoter in HEK 293T cells with constitutively active form of β-catenin (Δ90) and dominant negative (DN) TCF4. n.s.P>0.05. **(I)** Immunoblots for TDO2 and TCF4 in APC-KO MC38 cell lysates after transfecting with siControl or three different siTCF4s.

Fig. 3. TDO2-Kyn-AhR signaling is essential for cell survival in APC-mutated CRC cells. (A) Representative images of colony formation assays of APC-WT and APC-KO MC38 cell lines expressing shTDO2. Three independent experiments were performed.

(B) Quantification of Panel (A). **(C)** Immunoblots of cleaved caspase-3 in APC-WT and APC-KO MC38 cell lines with inducible shTDO2 after doxycycline (Dox) treatment. **(D)** Immunoblots for TDO2 and cleaved caspase-3 in $Apc^{Min/+}$ ishControl and ishTDO2 organoid cell lysates after Dox treatment for 48 h. Three independent experiments were performed. **(E)** Brightfield images of APC-WT and APC-KO colonoids treated with DMSO or TDO2 inhibitor (680C91). Scale bars, ×40 (50 μm). **(F)** Total flux measurement of tumors in Supplementary Fig. S4E. n.s.P>0.05, *P<0.05, **P<0.01. **(G)** Survival curves of C57BL/6J mice orthotopically implanted with ishTDO2 APC-WT and APC-KO MC38 cell lines (2×10^5 cells). Dox food was supplied at day 5 post-orthotopic injection to induce TDO2 knockdown in vivo. n.s.P>0.05; **P<0.01, ***P<0.001. Log-rank (Mantel-Cox) test. **(H)** Survival curves of C57BL/6J mice orthotopically implanted with APC-WT and APC-KO MC38 cell lines (2×10^5 cells). TDO2 inhibitor treatment (100 mg/kg) was initiated at day 5 post-injection twice a day by oral gavage. n.s.P>0.05, **P<0.01, ***P<0.001. Log-rank (Mantel-Cox) test. **(I)** Survival curves of iAP mice after tamoxifen induction in the distal colon. Vehicle or TDO2 inhibitor treatment (100 mg/kg) was initiated at day 24 post-induction once a day by oral gavage. Log-rank (Mantel-Cox) test.

Fig. 4. TDO2 mediates tumor growth by regulating macrophage infiltration. (A) GSEA analysis (Hallmark gene sets) on genes that overlap between RNA-seq datasets of ishTDO2 APC-KO MC38 cell lines (No dox vs. 48 hr dox, n=3) and microarray datasets of allograft tumors established with ishTDO2 APC-KO MC38 cell lines (No dox vs. dox treated, n=3). The blue bars indicate immune response-related pathways. RNA-

seq data from APC-KO MC38 ishTDO2 cell lines and tumor microarray datasets from the tumors established by the cell lines in C57BL/6J mice were overlapped and further narrowed down the list using the pathways that are upregulated by APC deletion to identify the pathways regulated both by WNT pathway and TDO2. **(B)** GSEA correlation of TNFA signaling and inflammatory response with alternatively expressed genes in TDO2-depleted APC-KO MC38 cells. Normalized enrichment scores (NES) and nominal P values are shown. **(C)** viSNE analysis of F4/80+ and CD206+ immune cells assessed by CyTOF from CRC orthotopic ishTDO2 APC-WT and APC-KO MC38 tumors. **(D)** Quantification of macrophages ($CD11b^+$ $F4/80^+$) and M2 macrophages ($CD11b^+$ $F4/80^+$ $CD206^{high}$) in $CD45^+$ cells from tumors shown in (C). CyTOF data were analyzed by FlowJo. Data represent mean ± s.d. n.s.P>0.05, *P<0.05. n=3 per group. **(E)** TDO2 mRNA expression significantly correlates with expression of total macrophage markers and M2 macrophage markers in TCGA CRC (COAD + READ, Provisional) patients (n=433). ****P<0.0001. **(F)** Representative images of IHC staining for CD163 in serial sectioned human CRC tumors with negative (n=42) and positive nuclear β-catenin (n=50). Scale bars, ×10 (200 μm) and ×20 (100 μm). **(G)** CRC tumors with nuclear β-catenin showed higher CD163 expression. Pearson Correlation Coefficient = 5.074, P =0.0243. Chi-squared test.

Fig. 5. TDO2-AhR-CXCL5 axis regulates macrophage recruitment in APC-mutated CRC tumors. (A) Expression of cytokine genes identified in RNA-seq analysis and TDO2 were validated by RT-qPCR using ishTDO2 APC-WT and APC-KO MC38 cell lines. **P<0.01, ***P<0.001, ****P<0.0001. **(B)** Volume of tumors established with

ishTDO2 APC-KO MC38 cell lines expressing Blank, CXCL5, CXCL7, and CSF3. Dox food was supplied at day 5 post-orthotopic injection to induce TDO2 knockdown in vivo. n=4 per group. n.s.P>0.05, *P<0.05, ****P<0.001, ****P<0.0001. **(C)** viSNE analysis of F4/80+ and CD206+ immune cells assessed by CyTOF from CRC orthotopic ishTDO2 APC-WT and APC-KO MC38 tumors and CXCL5-ORF expressing APC-KO MC38 with TDO2 depletion. **(D and E)** Quantification of macrophages ($CD11b^+$ $F4/80^+$) and M2 macrophages ($CD11b^+$ $F4/80^+$ $CD206^{high}$) in $CD45^+$ cells from tumors shown in (C). CyTOF data were analyzed by FlowJo. Data represent mean ± s.d., n.s.P>0.05, *P<0.05, **P<0.01, n=3 per group. **(F)** Representative images of migrated Raw264.7 cells cultured with ishTDO2 APC-WT and APC-KO MC38 conditioned media in transwell assay. Recombinant CXCL5 protein (50 ng) and SX-682 (1 μM) were added to harvested conditioned media for 36 hr. Scale bar, 100 μm. n=3 biological replicates. Quantification: n.s.P>0.05, ***P<0.001, ****P<0.0001. **(G)** Survival curves of C57Bl/6J mice orthotopically implanted with ishTDO2 and ishTDO2/CXCL5-ORF APC-KO MC38 cell lines (5×10^5 cells). Clondronate liposomes or control Encapsome liposomes were given intraperitoneally (100 μl) at day 2 post-orthotopic injection and three times a week. n.s.P>0.05, **P<0.01, ***P<0.001. Log-rank (Mantel-Cox) test.

Fig. 6. Graphical abstract

Fig. 1. TDO2 as a synthetic essential gene for mutant APC gene in CRC

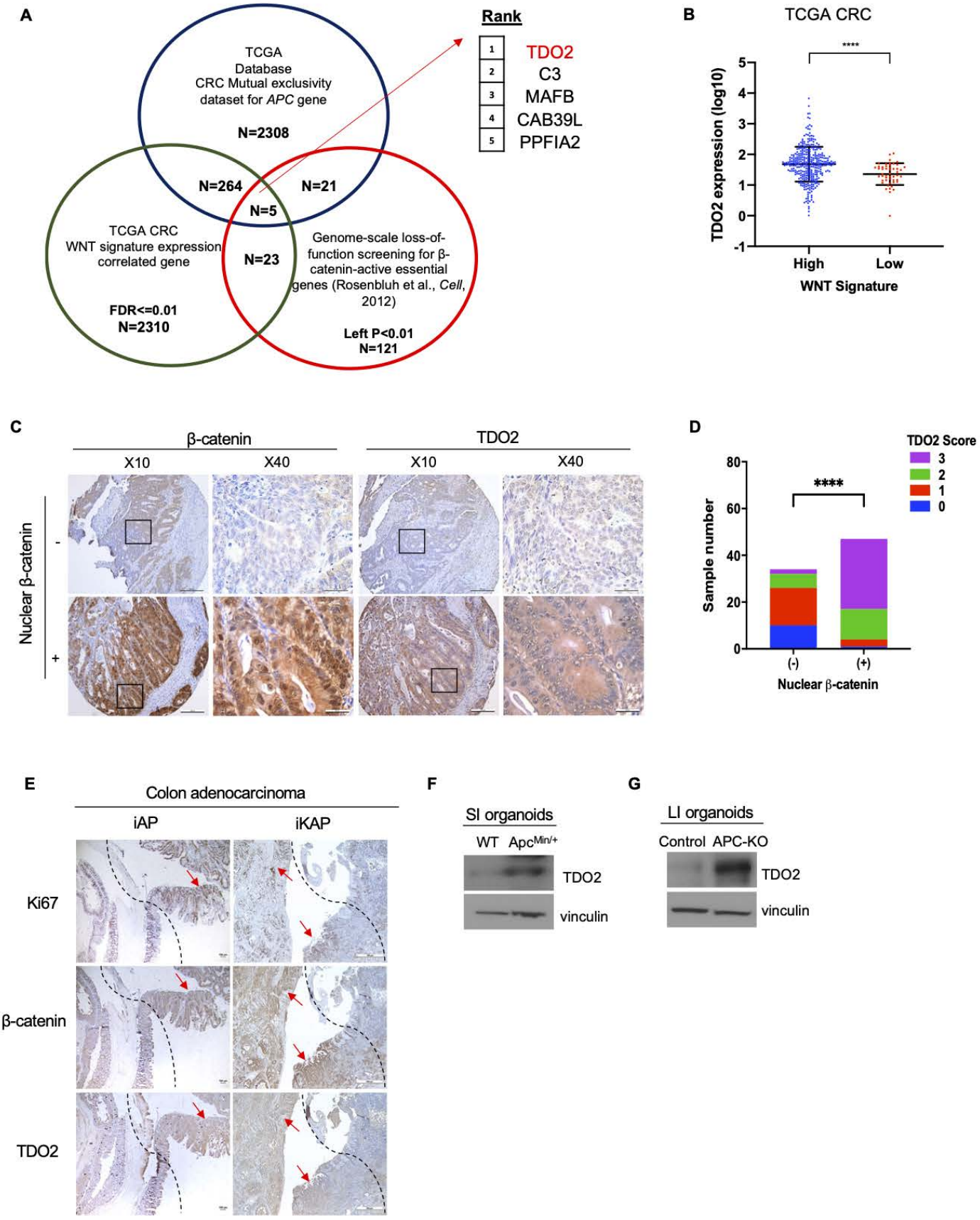

Fig. 2. TCF4(TCF7L2)/β-catenin mediates upregulation of TDO2 in APC-mutated CRC cells

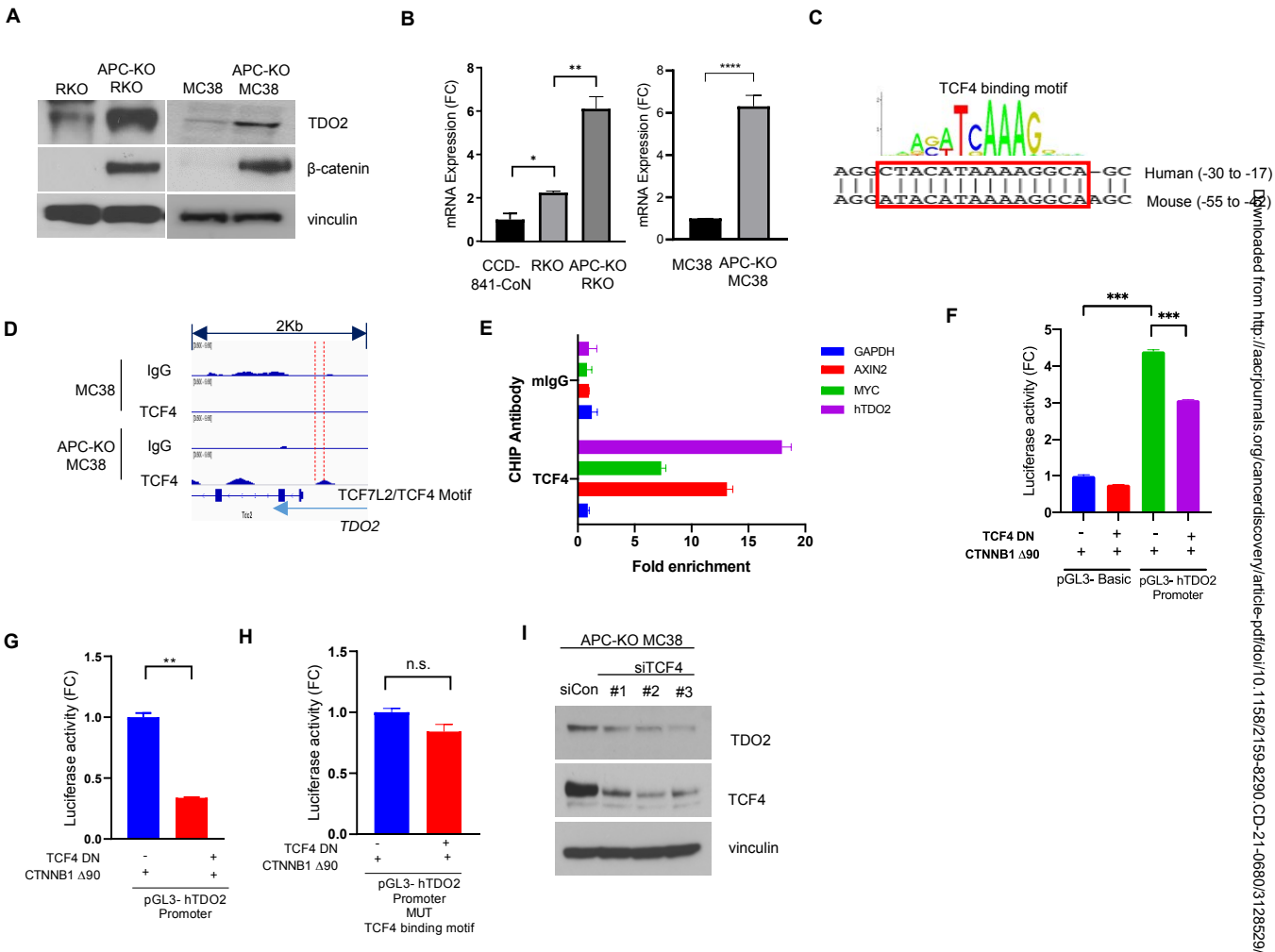

Fig. 3. TDO2-Kyn-AhR signaling is essential for cell survival in APC-mutated CRC cells

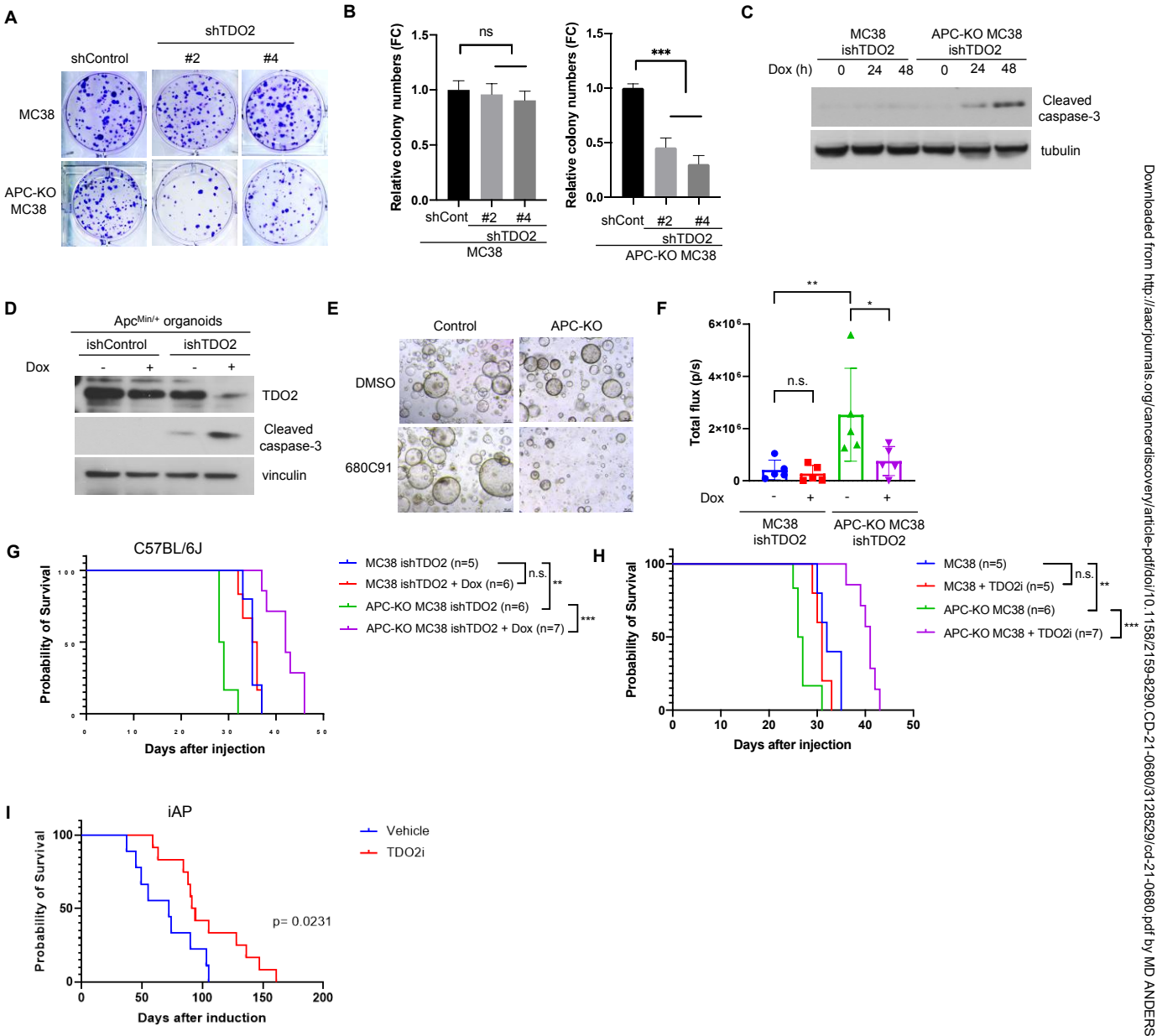

Fig. 4. TDO2 mediates tumor growth by regulating macrophage infiltration

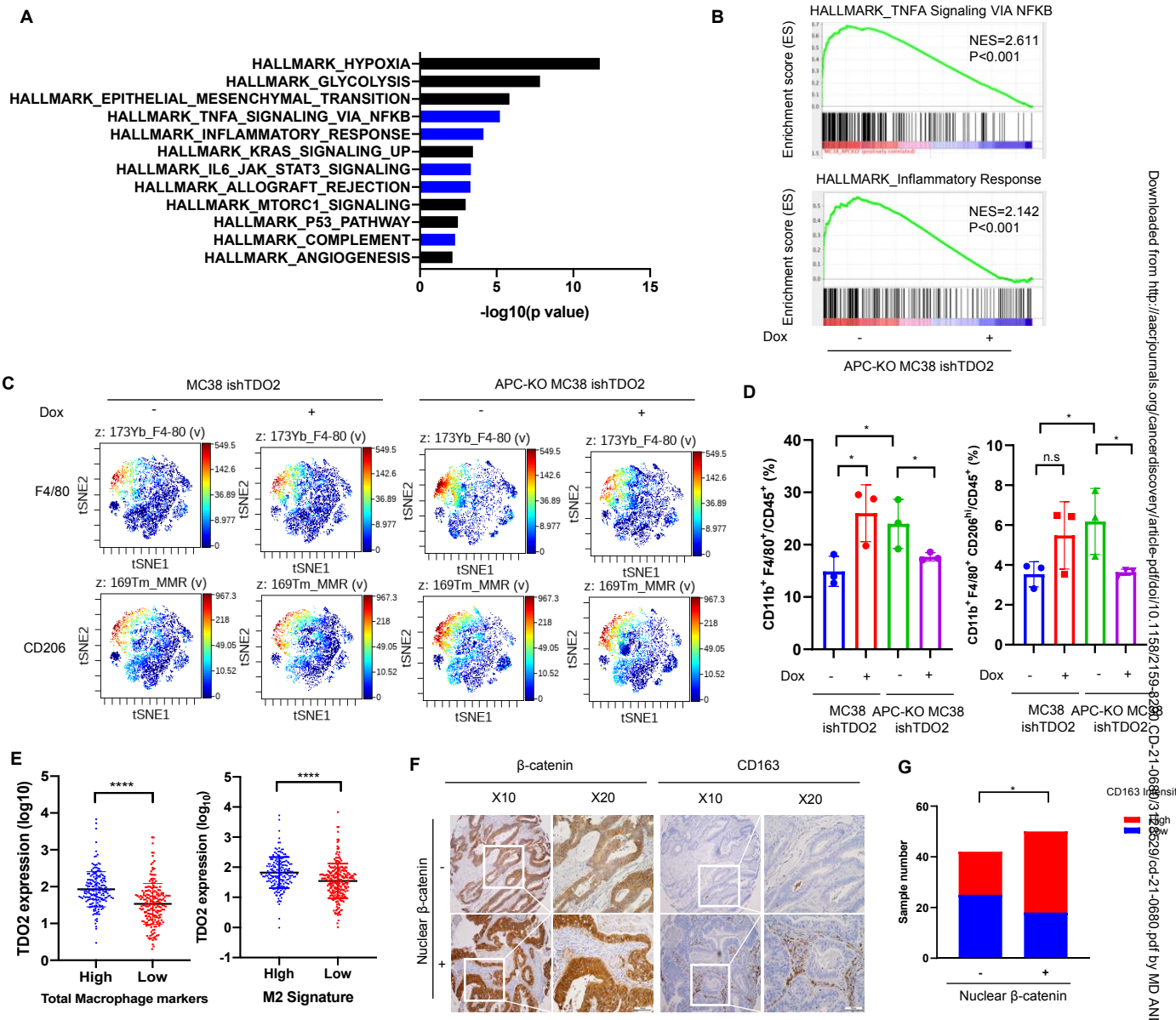

Fig. 5. TDO2-AhR-CXCL5 axis regulates macrophage recruitment in APC-mutated CRC tumors

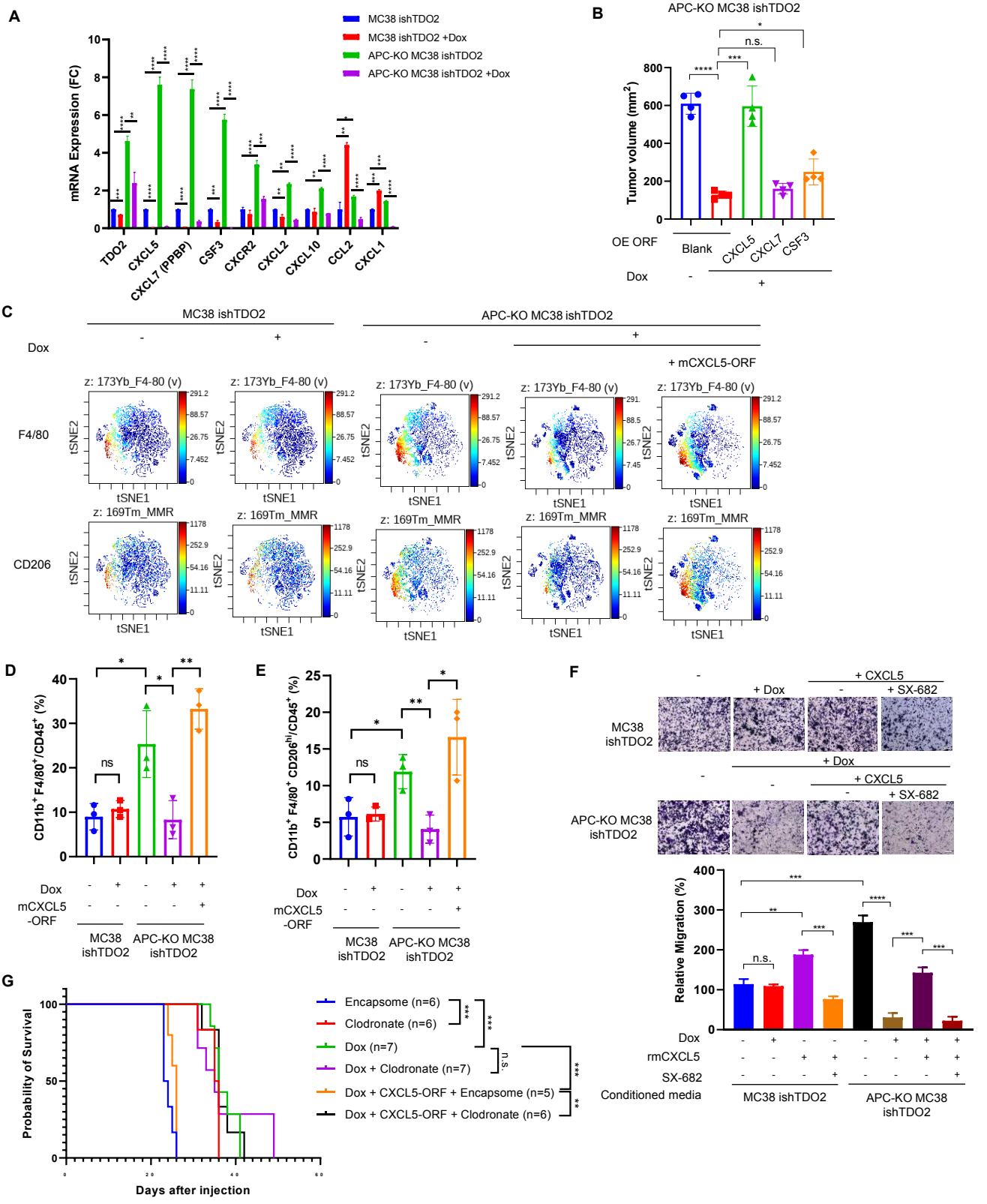

Fig. 6. Working model

A